Available online at www.sciencedirect.com
ScienceDirect
Journal of Hazardous Materials 151 (2008) 17–25
Journal of Hazardous Materials
www.elsevier.com/locate/jhazmat

Photocatalytic oxidation of nitric oxide with immobilized titanium dioxide films synthesized by hydrothermal method

Zhongbiao Wu, Haiqiang Wang, Yue Liu *, Zhuoliang Gu

Department of Environmental Engineering, Zhejiang University, Hangzhou 310027, China

Received 26 December 2006; received in revised form 9 April 2007; accepted 15 May 2007
Available online 21 May 2007

Abstract

Gas-phase photocatalytic oxidation (PCO) of nitric oxide (NO) with immobilized TiO_2 films was studied in this paper. The immobilized TiO_2 films were synthesized by hydrothermal method. The characterization for the physicochemical properties of catalysts prepared under different hydrothermal conditions were carried out by X-ray diffraction analysis (XRD), transmission electron microscopy (TEM), high resolution-transmission electron microscopy (HR-TEM), Brunauer–Emmett–Teller measurements (BET) and scanning electron micrograph (SEM). It was found that the PCO efficiency of the catalyst was mainly depended on the hydrothermal conditions. The optimal values of hydrothermal temperature and hydrothermal time were 200 °C and 24 h, respectively. Furthermore, it was also known that the photocatalytic efficiency would decrease remarkably when the calcination temperature was over than 450 °C. Under the optimal conditions (hydrothermal condition: 200 °C for 24 h; calcination temperature: 450 °C), the photocatalytic efficiency of catalyst could reach 60% higher than that of Degussa P25.

Keywords: Photocatalytic oxidation; Nitric oxide; Immobilized titanium dioxide; Hydrothermal method; Crystallization

1. Introduction

Nitrogen oxides (NOx) emissions to the air have direct impact on the global environment and human health through the formation of photochemical smog and the acid deposition. Various processes, including combustion modifications, dry processes and wet processes have been developed to remove NO from flue gas [1–6].

Traditional wet processes are very efficient to remove NO_2 from flue gas, but cannot remove NO because of its low solubility in aqueous solution [7–10]. One promising approach to improve the absorption efficiency of wet processes is the transformation of NO to NO_2 by the gas-phase oxidation.

The photocatalytic oxidation (PCO) may be an environmentally friendly and cost-effective process to convert NO to NO_2 in gas-phase [11,12]. The PCO of NOx in the ambient atmosphere, using TiO_2 as the photocatalyst, was firstly reported in 1994 [13]. Ichiura et al. studied the PCO of nitrogen oxides over titanium dioxide sheets that contained metal compounds [14]. Dalton et al. investigated the NOx adsorbate reaction at the TiO_2 substrate surface in the PCO [15]. Hashimoto et al. reported the PCO of NO with Hycom TiO_2 and zeolite to remove NOx in the atmosphere [16]. Devahasdin et al. [17] studied the mechanism for the PCO of NO. It was found in his study that the PCO behavior consisted of a series of oxidation steps by the $OH^{\bullet}$ radical and O_2^-.

Unfortunately, the mentioned investigations were mostly focused on the removal of NO from ambient environment (either indoor or outdoor air). Comparing with NOx from flue gas, the concentration of NO from ambient environment is much lower. Therefore, it is necessary to develop more effective ways to enhance the photocatalytic efficiency at high concentration of NO for the treatment of NO from flue gas. In general, a large surface area and good crystallinity of catalysts are beneficial to the TiO_2-based photocatalysis in air phase [11,16,17]. The hydrothermal method has been found to be one of the best techniques to prepare TiO_2 particles of desired size and shape with homogeneity in composition as well as a high degree of crystallinity [18–21]. Its most important feature is that it favors a decrease in agglomeration among particles, narrow particle size distributions, phase homogeneity and controlled particle morphology.

* Corresponding author. Tel.: +86 571 87952459; fax: +86 571 87953088.
E-mail address: yueliu@zju.edu.cn (Y. Liu).

0304-3894/$ – see front matter © 2007 Elsevier B.V. All rights reserved.
doi:10.1016/j.jhazmat.2007.05.050

In this study, several TiO_2-based catalysts were prepared by hydrothermal method and NO conversion was investigated in the presence of air under light irradiation. The effect of hydrothermal conditions on the NO conversion efficiency was studied. The physicochemical properties of the prepared TiO_2 catalysts were characterized and the relationship between physicochemical properties and NO conversion efficiency were discussed.

2. Experimental

2.1. Material

NO gas from a compressed gas cylinder with a nitrogen balance was used for the NO oxidation experiments (concentration: 10,000 ppm). The Degussa P25 TiO_2 powder was obtained from Degussa (crystal size: 20–50 nm, surface area: $50 \pm 5\ m^2/g$, crystal distribution: 70% anatase and 30% rutile). Tetrabutyl titanate, ethanol and distilled water were all analytical grade. The woven glass fabric was supplied by Hangzhou woven glass fabric factory (thickness: 0.5 mm; filament diameter: 9 μm).

2.2. Preparation of TiO_2 catalysts

Nano-sized TiO_2 was prepared by hydrothermally treating the sol–gel derived hydrous oxides [19]. 0.1 mol tetrabutyl titanate was dissolved in 1.5 mol anhydrous ethanol and the prepared solution was then added dropwise to a water–ethanol solution containing 1 mol ethanol until the ratio of water to tetrabutyl titanate reach 50. A white precipitate of amorphous oxide was produced and the mixture was stirred by a magnetic stirrer at room temperature for 1 h. Then the precipitate and mother-liquid were transferred to a Teflon-covered stainless steel autoclave (volume: 100 ml). The autoclave was then placed in a furnace for the hydrothermal treatment (temperature: 120–240 °C, time: 1–24 h). After hydrothermal crystallization, the precipitate was washed by ethanol three times followed by centrifugation. Then the collected particles were diffused into anhydrous ethanol to make 5% (w/w) suspension for the next dip-coating process.

Immobilization was carried out by the dip-coating method. The TiO_2 suspension was gradually dropped and the catalyst was coated on the woven glass fabric (pretreatment: 500 °C for 1 h) over an area of 4 cm × 80 cm. The coated woven glass fabric was treated with a desiccation process in a convection oven at 80 °C overnight. Finally, the woven glass fabric was calcined at different temperatures ranged from 200 to 750 °C for 3 h. The amount of TiO_2 coated was determined as the mass increase of the woven glass fabric after the coating. In all experiments, the weight of TiO_2 coated was determined to be $0.5\ g \pm 10\%$.

2.3. Characterization of TiO_2 catalysts

X-ray diffraction analysis (XRD) of the catalysts was performed on a Rigaku diffractometer (D/Max RA) at 40 kV and 150 mA, at an angle of 2θ from 20° to 80°. The scan speed was 1°/min. The strongest TiO_2 peaks, corresponding to anatase (1 0 1) and rutile (1 1 0), were selected to evaluate the crystallinity of the samples. The mean crystallite size was determined by the Scherrer equation. Brunauer–Emmett–Teller measurements (BET), with nitrogen as the adsorption molecule (ASAP 2020, Micromeritics Com.), were used to determine the surface area of the samples. The morphology, structure and grain size of TiO_2 particle were examined by transmission electron microscopy (TEM) and high resolution-transmission electron microscopy (HR-TEM) using a JEM-2010 instrument. Microstructures of the prepared samples, after being coated with platinum, were observed with a scanning electron micrograph (SEM) in Phillips XL-30-ESEM system at a voltage of 20 kV.

2.4. Experimental set-up

A set of experiments for the removal of NO from a gaseous phase was carried out in the continuous-flow reactor using the catalysts prepared under different conditions. The experimental set-up consisted of the gas supply, PCO reactor and analytical system [22]. The air, NO and N_2 gas streams were mixed to obtain the desired concentration (NOx: 90 ppm; NO: 80 ppm; relative humidity: 80%). The flow rate of the gas was 2.0 L/min and the empty bed retention time (EBRT) was 10 s.

The immobilized catalyst was set into a Pyrex reactor with "Z" type. The Pyrex reactor was irradiated with one Hg-arc lamp (125 W, Philips) outside, with a volume of 340 ml. The wavelength of the Hg-arc lamp varied in the range from 300 to 400 nm with the maximum light intensity at 365 nm. The Pyrex reactor and light source were set in a hollow chamber that was coated with tinfoil. The temperature of the reactor and lamp were controlled by the fan. The reaction temperature in the reactor was 80 ± 5 °C, heated by the irradiation of the Hg-arc lamp. NO, NO_2 and O_2 were measured with a Kane International Limited Model KM-9106 flue gas analyzer. The relative humidity was measured with a relative humidity analyzer (Testo Co. Ltd., Model 605-H1).

The blank test consisted of a gas stream of ca. 90 ppm NOx (ca. 80 ppm NO) that was irradiated by the Hg-arc lamp, without the TiO_2 photocatalyst, at 80 ± 5 °C. The variation of the NO concentration could not be observed within 120 min irradiation. Moreover, there was also no change of the NO concentration in the inlet or the outlet when the Hg-arc lamp was turned off and the catalyst was present in the reactor. Therefore, it was concluded that the absence of the TiO_2 or the Hg-arc lamp does not cause the oxidation of NO.

3. Result and discussion

3.1. Crystal structure and size of TiO_2 catalysts

A series of TiO_2 catalysts with different hydrothermal temperatures at 120, 160, 200 and 240 °C was prepared and named as HT-120, HT-160, HT-200 and HT-240, respectively. The hydrothermal time of the mentioned catalysts was 12 h and the calcination temperature was 450 °C. The XRD patterns of catalysts with different hydrothermal temperature were shown in Fig. 1. The results of XRD analysis indicated that the catalysts were anatase structure. The crystal size of these catalysts was determined by the Scherrer equation to be in the range between

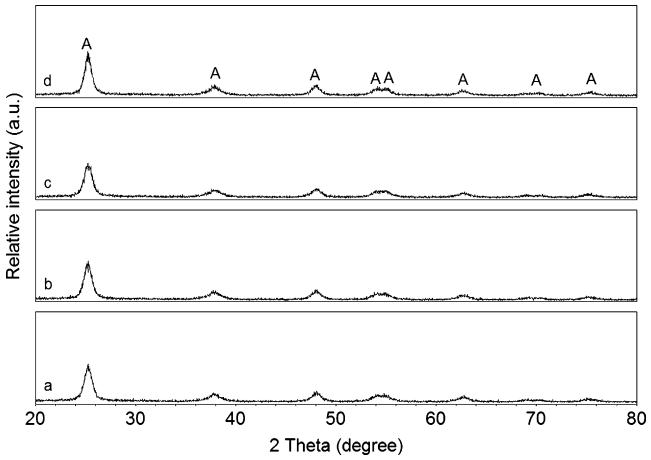

Fig. 1. XRD patterns of catalysts with different hydrothermal temperatures ((a) HT-120; (b) HT-160; (c) HT-200 and (d) HT-240).

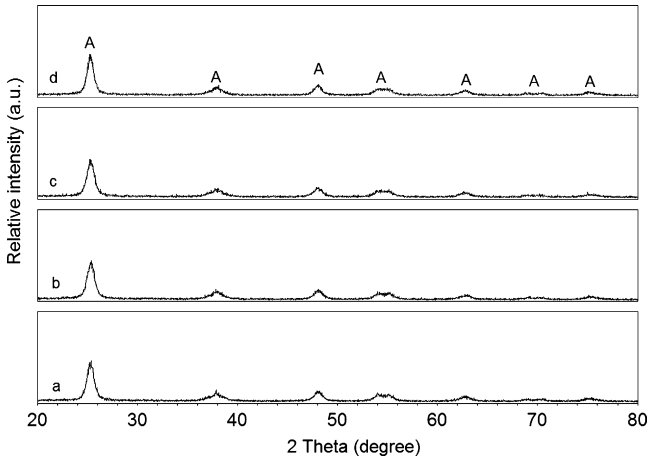

Fig. 2. XRD patterns of catalysts with different hydrothermal times ((a) HH-1; (b) HH-6; (c) HH-12 and (d) HH-24).

7.4 and 8.4 nm as listed in Table 1. The amounts of rutile phase formed in the heated samples were calculated from the following equation [23]: $F_R = 1/\{1 + 0.79\ [I_A(1\,0\,1)/I_R(1\,1\,0)]\}$. Here F_R is the mass fraction of rutile in the samples; I_A (1 0 1) and I_R (1 1 0) are the integrated 1 0 1 intensities of anatase and 1 1 0 of rutile, respectively.

These results showed that the hydrothermal temperature did not have significant influence on the crystal size. The crystallinity of TiO_2 nanoparticles could be evaluated via the relative intensity of the (1 0 1) diffraction peak of the anatase [24,25]. Further observation with XRD patterns revealed that with an increase in hydrothermal temperatures (range: 120–240 °C), XRD peak intensities of anatase became stronger and the width of XRD diffraction peaks of anatase became slightly narrower, indicating the formation of more TiO_2 crystallites and an enhancement of crystallization.

The catalysts with different hydrothermal times at 1, 6, 12 and 24 h were prepared and named as HH-1, HH-6, HH-12 and HH-24, respectively. The hydrothermal temperature of the mentioned catalysts was 200 °C and the calcination temperature was 450 °C. The XRD patterns of catalysts with different hydrothermal time were presented in Fig. 2. The results of XRD analysis indicated that the catalysts were anatase structure.

The crystal size of these catalysts was determined by the Scherrer equation to be between 8.9 and 7.6 nm as listed in Table 1. From Table 1, it was shown that the hydrothermal time had little influence to the crystal size of TiO_2. Further observation revealed that the crystal size had a slight decrease at the initial stage of hydrothermal treatment. This could be attributed to the growth rules of TiO_2 crystallites under hydrothermal conditions [26]. At low temperature (up to around 300 °C) a solid state epitaxial growth mechanism dominated, and a dissolution/precipitation mechanism dominated above this temperature. When the solid state epitaxial growth mechanism dominated, the crystal size would not increase rapidly. Thus, the crystal sizes had negligible variations with lower hydrothermal temperatures.

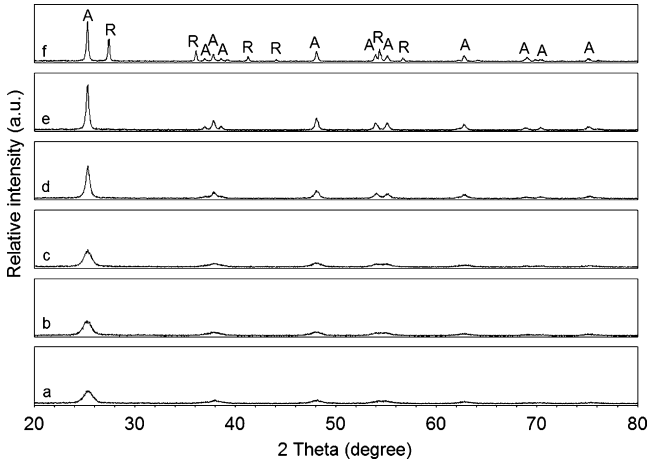

Fig. 3. XRD patterns of catalysts with different calcination temperatures ((a) HC-200; (b) HC-350; (c) HC-450; (d) HC-550; (e) HC-650 and (f) HC-750).

The catalysts with different calcination temperatures at 200, 350, 450, 550, 650 and 750 °C were prepared and named as HC-200, HC-350, HC-450, HC-550, HC-650 and HC-750, respectively. The hydrothermal temperature of the mentioned catalysts was 200 °C and the hydrothermal time was 12 h. The XRD patterns of catalysts with different calcination temperatures were presented in Fig. 3. The crystal size of these catalysts was determined by the Scherrer equation to be between 6.4 and 81.1 nm as list in Table 2.

Table 1
Physical properties of TiO_2 with different hydrothermal temperatures and times

Catalyst code	HT-120	HT-160	HT-200	HT-240	HH-1	HH-6	HH-12	HT-24
Crystal phase	Anatase	Anatase	Anatase	Anatase	Anatase	Anatase	Anatase	Anatase
Crystal size (nm)	7.4	7.7	7.6	8.4	8.9	8.3	7.6	7.6

Table 2
Physical properties of TiO_2 with different calcination temperatures

Items	Catalyst					
	HC-200	HC-350	HC-450	HC-550	HC-650	HC-750
Calcination temperature (°C)	200	350	450	550	650	750
Anatase (%)	100	100	100	100	100	61.8
Crystallite size (nm)	6.4	7.9	7.6	15.9	28.5	51.3
Rutile (%)	–	–	–	–	–	38.2
Crystallite size (nm)	–	–	–	–	–	81.1
One point BET surface area (m^2/g) ($P_s/P_0 = 0.3$)	140.97	116.51	127.44	60.28	26.84	12.68
BET surface area (m^2/g)	148.50	119.23	131.25	62.46	27.57	13.13
Single point adsorption total pore volume of pores ($P_s/P_0 = 0.3$) (10^{-2} cm^3/g)	7.16	5.92	6.47	3.08	1.36	0.64

The results of XRD analysis indicated that the catalysts were anatase structure except HC-750. It could be seen that the peak intensities of anatase increased greatly and the width of the (1 0 1) plane diffraction peak of anatase became narrower with increasing calcination temperature. The crystal size increased slightly when the calcination temperature was lower than 450 °C, but it increased rapidly with the higher calcination temperature. It could be also found that the rutile structure did not appear in the catalysts until the calcination temperature reached 750 °C.

3.2. Microstructure and crystallization analysis by TEM and HR-TEM

TEM and HR-TEM were used to study the microstructures and crystallization of the hydrothermal treated TiO_2 powders. TEM micrographs of HT-200, HT-120, HH-12 and HH-1 were shown in Fig. 4. From the TEM micrograph of HT-200, shown in Fig. 4a, it could be seen that the primary particle size was about 7 nm, which was in agreement with the value of the crystallite size determined by XRD (7.6 nm, as shown in Table 1). Furthermore, it could be found that HT-200 had a well crystallinity of TiO_2 (shown by the arrowhead). Fig. 4b showed the TEM image of the TiO_2 powders prepared at 120 °C for 12 h (HT-120). The crystal profiles were somewhat unclear and ambiguous; the crystal size was lack of homogeneity (shown by the arrowhead). From Fig. 4a and b, it could be known that the crystal profile of HT-200 was clearer than that of HT-120. It indicated that a high hydrothermal temperature could enhance the crystallinity of TiO_2, which was in agreement with the result of XRD analysis. Similar results were obtained from Fig. 4c and d that a long hydrothermal time would enhance the crystallinity of TiO_2.

HR-TEM micrographs of HT-200, HT-120, HH-12 and HH-1 were shown in Fig. 5. From Fig. 5a clear lattice fringes could be observed, which allowed the identification of crystallographic spacing and indicated the prepared anatase TiO_2 powder was well crystalline. The lattice fringes of 0.352 nm were corresponding to the crystallographic planes (1 0 1) of anatase TiO_2 [27,28]. From Fig. 5a, the lattice fringes of anatase (1 0 1) plane were calculated to be 0.350 nm, which matched the mentioned value (0.352 nm) well. From the HR-TEM photograph of HT-120 shown in Fig. 5b, it could be found the crystals had abnormity shape. The crystal profiles and fringes were unclear and the calculated lattice fringes of anatase (1 0 1) plane were 0.325 nm. The result confirmed the conclusion gained from the TEM analysis.

The HR-TEM photograph of HH-12 shown in Fig. 5c showed better crystallinity compared with those shown in Fig. 5d. In Fig. 5c the grain boundary and the lattice fringe could be observed obviously, and the single crystal grain size was about 10 nm. The straight fringes were observed in the grains, and the lattice fringes corresponding to the anatase (1 0 1) were measured as 0.354 nm. Furthermore, the calculated lattices of (1 0 1) plane for HH-1 were measured as 0.335 nm. All these results demonstrated that the surface of (1 0 1) for HH-12 was more perfect than HH-1.

3.3. Surface area and pore size of TiO_2 catalysts

The specific surface area, *t*-plot total surface area and total pore volume ($P_s/P_0 = 0.3$) of TiO_2 samples were measured by the BET method. The analytical results for the TiO_2 catalysts prepared at different calcination temperatures were listed in Table 2.

The results in Table 2 indicated that the TiO_2 samples prepared by the hydrothermal method had the large total surface area and total pore volume. It was shown that total surface area and total pore volume had a little change when the calcination temperature was lower than 450 °C. However, a higher calcination temperature (>450 °C) would do harm to the surface morphology of TiO_2, because the total surface and total pore volume would decrease rapidly when the calcination temperature was higher than 450 °C.

3.4. Microstructure and morphology of immobilized TiO_2 films

SEM studies were conducted to investigate microstructure and morphology of immobilized TiO_2 films. Fig. 6 showed SEM micrographs of sample HC-200 and HC-650.

After thermal treatment at 200 °C and for 3 h, there were lots of crystals with small size in the films, the surface was very smooth; and TiO_2 particles were well-dispersed, the surface of the film was uniform with free crack (Fig. 6a and b, for HC-200). As the calcination temperature increased (650 °C), the size of crystals enlarged and crystals dispersion became disorderly

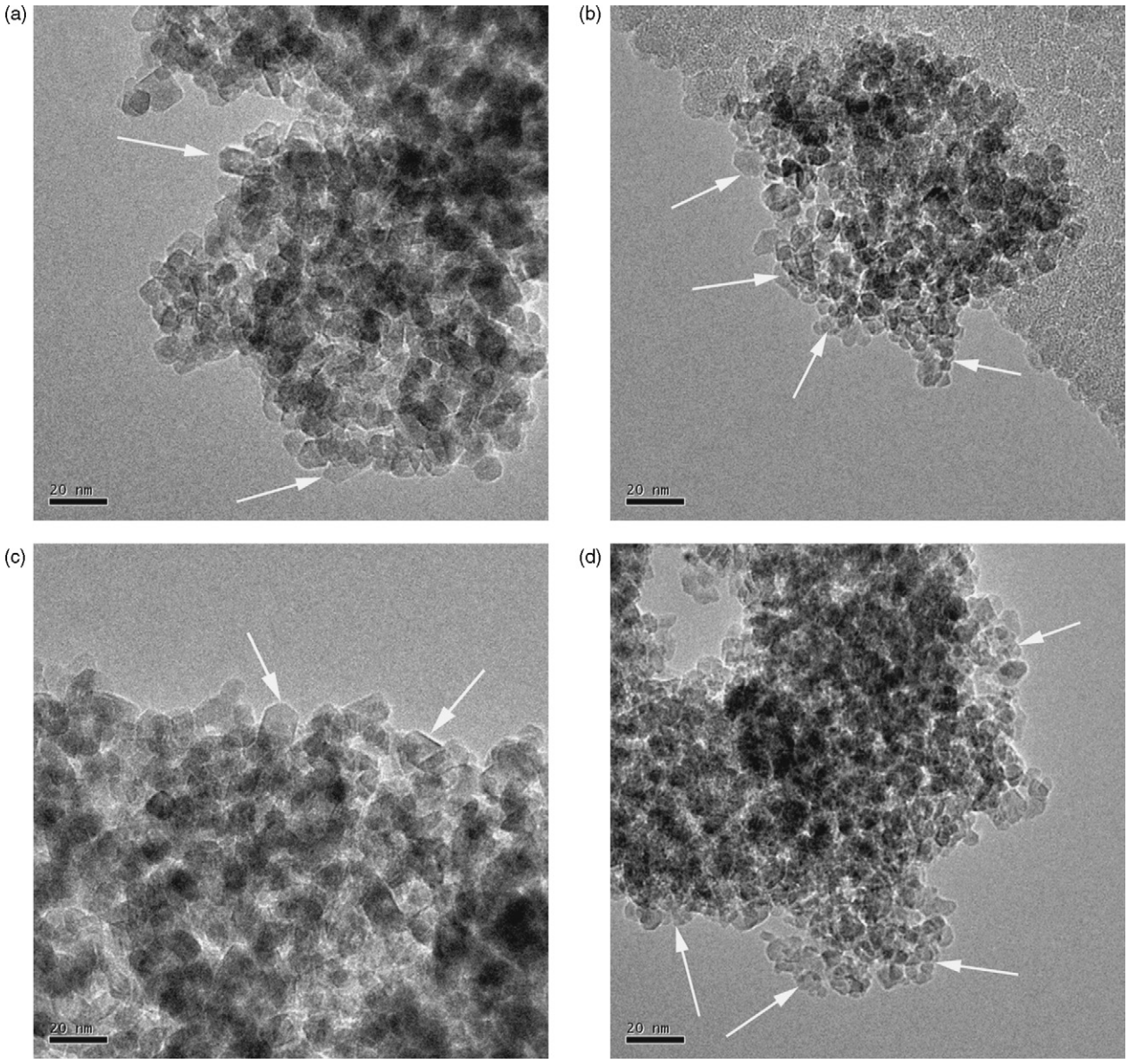

Fig. 4. TEM micrographs of TiO_2 particles ((a) TEM of HT-200; (b) TEM of HT-120; (c) TEM of HH-12 and (d) TEM of HH-1).

in Fig. 6c and d, and the evident cracks could be seen in the TiO_2 films. Also, it could be seen the visible aggregates of TiO_2 particles on the film surface. The results agreed well with the conclusions from XRD and BET analysis that the high calcination temperature would lead to the aggregate of TiO_2 particle and destroy the surface of catalyst.

3.5. NO conversion

Experimental study to remove NO from a gaseous phase was carried out in a continuous-flow reactor using different catalysts. After a stabilized period for about 1 h, outlet NO concentration became the same as that of inlet gas and then the experiment started by turning on the UV lamp. The PCO behavior consisted of a series of oxidation steps by the $OH^{\bullet}$ radical and O_2^-: $NO \rightarrow HNO_2 \rightarrow NO_2 \rightarrow HNO_3$ [17,22]. At steady-state, the equilibrium between HNO_3 and NO_2 was reached on the catalyst surface. NO_2 was the dominant product at the steady-state. In this experiment, the steady-state was defined as the situation after 120 min reaction, since the variation of the outlet concentration of the NO was less than 5%. The NO conversion of steady-state was calculated according to the definition as: NO conversion = (([NO]inlet − [NO]outlet)/[NO]inlet) × 100.

Fig. 7 showed that variation of the NO conversion of catalysts with different hydrothermal temperatures and Degussa P25. For the catalysts of HT-120, HT-160, HT-200, HT-240 and Degussa P25, the conversion of NO at the steady-state was 50.6, 65.4, 68.7, 71.1 and 48.0%, respectively. From Fig. 7, it could be found that the catalysts prepared with the different hydrothermal temperatures had good photocatalytic activities for NO oxidation except HT-120. HT-240 had the best photocatalytic activity among the mentioned catalysts, which was 1.5 times higher than Degussa P25. From the result of XRD analysis (Fig. 1), it was obviously shown that hydrothermal

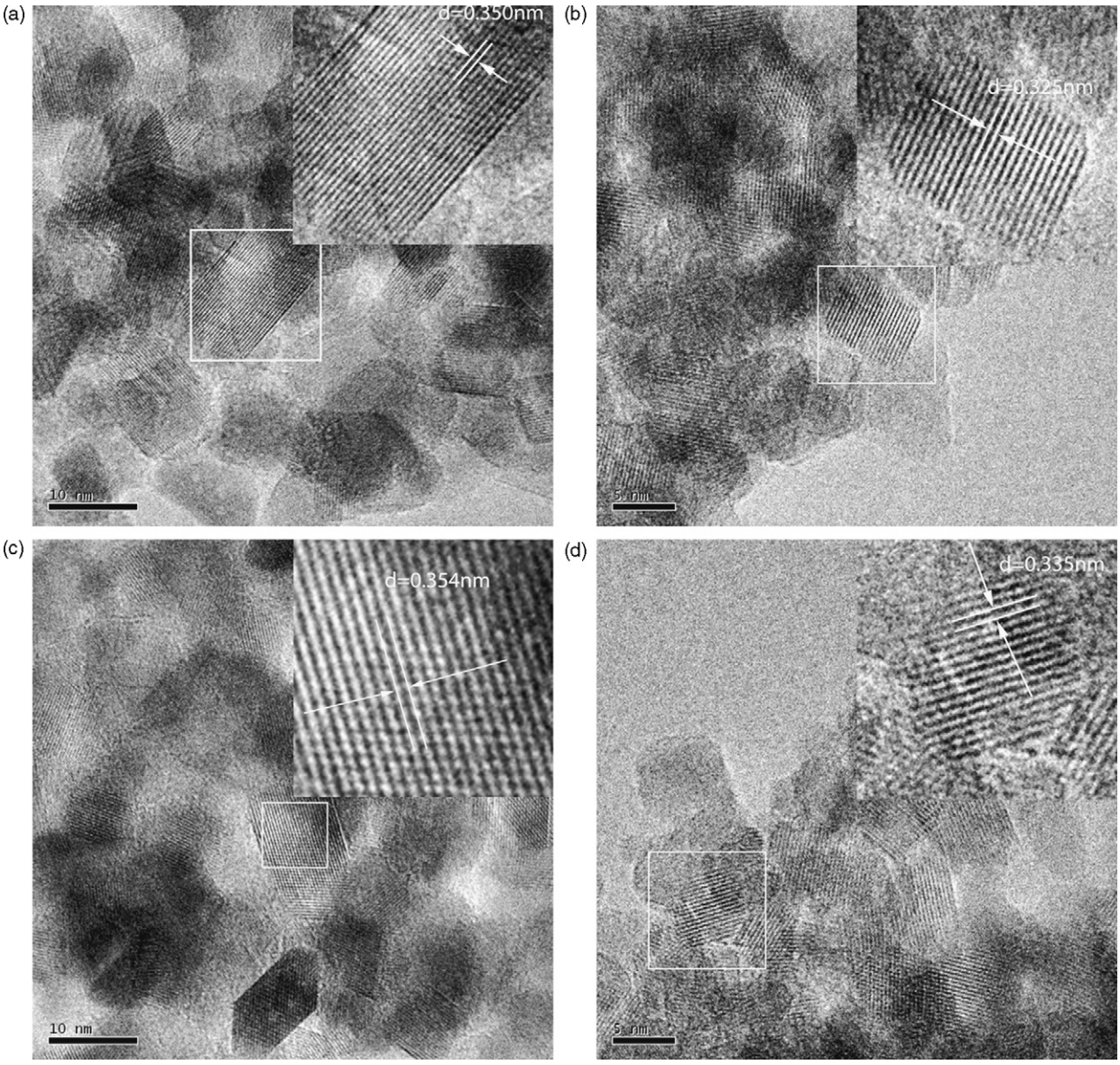

Fig. 5. HR-TEM micrographs of TiO_2 particles ((a) HR-TEM of HT-200; (b) HR-TEM of HT-120; (c) HR-TEM of HH-12 and (d) HR-TEM of HH-1).

temperature had little influence on the crystal size of TiO_2. However, from the TEM and HR-TEM analysis (Figs. 4 and 5) it indicated that the catalysts with high hydrothermal temperature (>160 °C) had a better degree of crystallinity than others. Previous studies [19,24,29] also gave the similar conclusions. From Fig. 7, higher hydrothermal temperature could not give obvious increase of NO conversion efficiency when hydrothermal temperature was over than 200 °C. In view of the energy cost, the suitable hydrothermal temperature should be around 200 °C.

Fig. 8 showed that variation of the NO conversion of catalysts with different hydrothermal times. It could be seen from Fig. 8 that the NO conversion increased with an increase in hydrothermal times. For the catalysts of HH-1, HH-6, HH-12 and HH-24, the conversion of NO at steady-state was 60.7, 70.0, 68.7 and 73.8%, respectively (Fig. 8). From the result of XRD analysis (Fig. 2), it was shown that hydrothermal time had little influence on the crystal size of TiO_2. However, TEM and HR-TEM analyses (Figs. 4 and 5) had indicated that the long hydrothermal temperature (>12 h) led to a high degree of crystallinity. Therefore, the catalyst had a better photocatalytic activity with a longer hydrothermal time.

Fig. 9 showed that variation of the NO conversion of catalysts with different calcination temperatures. The conversion of NO for the catalysts (HC-200, HC-350, HC-450, HC-550, HC-650 and HC-750) at steady-state was 76.0, 70.7, 68.7, 25.3, 19.5 and 13.8%, respectively (Fig. 9). It could be seen that the photocatalytic activity of the TiO_2 decreased fast when the calcination temperature was higher than 450 °C. From the analysis of XRD, it was observed that the crystal size increased fast with the high calcination temperature (>450 °C). The total surface and total pore volume decreased greatly for a higher calcination temperature (see Table 2). Therefore, too higher calcination temperature (>450 °C) would damage the surface morphology of TiO_2, leading to an obvious reduction of NO conversion.

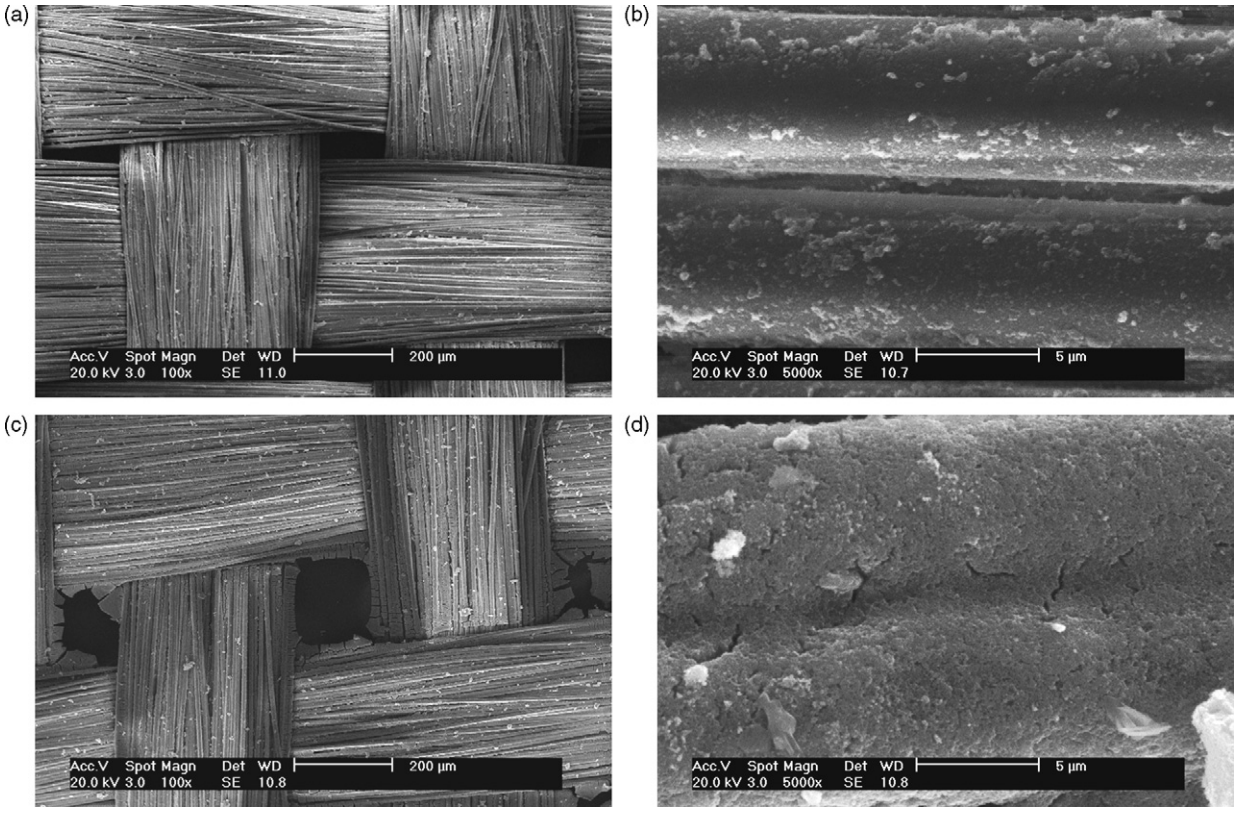

Fig. 6. SEM micrographs of TiO_2 particle films ((a) HC-200, 100×; (b) HC-200, 5000×; (c) HC-650, 100× and (d) HC-650, 5000×).

Deng et al. [19] and Kominami et al. [30] reported that the activity of their hydrothermally produced titania photocatalysts improved when they were calcined. The enhancement of photocatalytic activity might be attributed to the reduction of organic residues [19] or the decrease in the number of crystallite defects in the powder [30]. In our cases, it was clear that the catalyst with low calcination temperature had the better efficiency within the investigated range. It might be thought that low calcination temperature of 200 °C was sufficient to reduce the organic residues on TiO_2 particles. Furthermore, the calcination temperature (under 450 °C) would have little influence on the physical properties of TiO_2 (Table 2). But the high calcination temperature (>550 °C) had a devastating influence on the surface areas of catalysts, leading to the reduction of activity. The similar results could be also found in the literature [26]. Thus, it was confirmed that the calcination temperature under 450 °C was more adequate for the hydrothermal preparation of TiO_2.

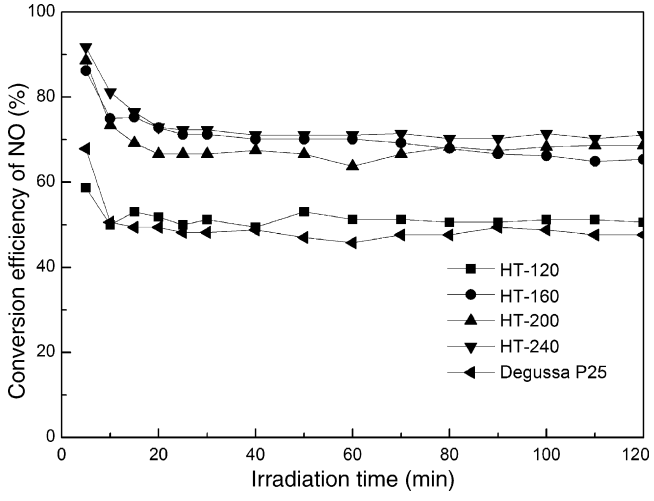

Fig. 7. NO conversion efficiency of catalysts with different hydrothermal temperatures (125 W Hg-arc lamp; relative humidity: 80%; O_2 concentration: 21%; EBRT: 10 s).

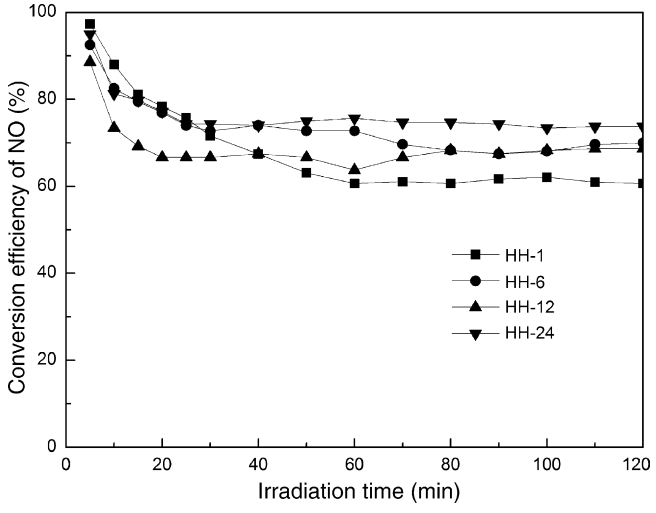

Fig. 8. NO conversion efficiency of catalysts with different hydrothermal times (125 W Hg-arc lamp; relative humidity: 80%; O_2 concentration: 21%; EBRT: 10 s).

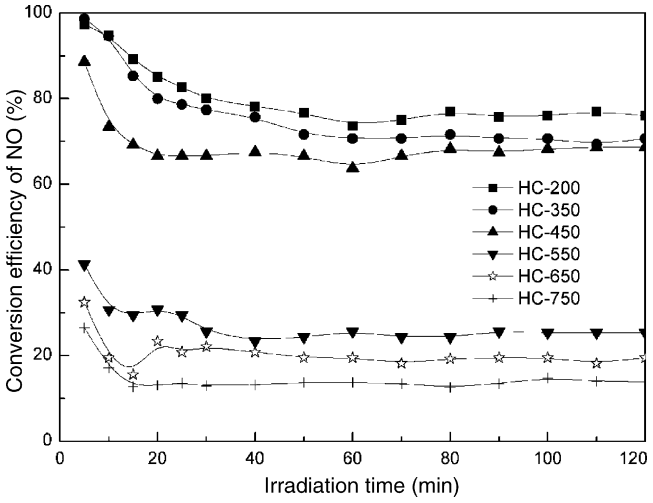

Fig. 9. NO conversion efficiency of catalysts with different calcination temperatures (125 W Hg-arc lamp; relative humidity: 80%; O_2 concentration: 21%; EBRT: 10 s).

Comparing the photocatalytic activity between the TiO_2 powders with different hydrothermal treatment and Degussa P25, it could be seen that the catalysts with hydrothermal treatment had better photocatalytic activity than Degussa P25. Under the optimal conditions, the photocatalytic activity of catalyst (HC-200) was 1.6 times as high as Degussa P25. It was well known that the photocatalytic activity of TiO_2 depended upon its crystal structure (anatase, or rutile), surface area, size distribution, porosity, presence of dopants, and surface hydroxyl group density, etc. These factors influenced directly on the production of electron–hole pairs, the surface adsorption and desorption process and the redox process [11,18]. From the result of XRD analysis, it was observed that TiO_2 particles prepared by hydrothermal method had a small crystal size, narrow particle size distribution, pure anatase phase and a high degree of crystallinity compared to the TiO_2 particles prepared by other methods [19,24,31,32]. TEM micrographs, HR-TEM micrographs and SEM micrographs indicated these excellent properties of TiO_2 prepared by hydrothermal treatment. Furthermore, BET analysis indicated that these particles had a large surface area as three times as Degussa P25. The high photocatalytic activity of the particles might be attributed to these excellent characters.

4. Conclusion

Immobilized TiO_2 particle films with high photocatalytic activity for the NO oxidation were prepared by a hydrothermal method. The effect of hydrothermal conditions (hydrothermal temperature, hydrothermal time and calcination temperature) on the TiO_2 particle characters and NO conversion efficiency was studied. It could be drawn from this study that:

(1) Compared to other methods, TiO_2 particle films prepared by hydrothermal method had a small crystal size (7–10 nm), narrow particle size distribution, pure anatase phase and a high degree of crystallinity;
(2) with the increasing of hydrothermal temperature or time, the degree of crystallinity could be improved. For the photocatalytic oxidation of NO, hydrothermal temperature (around 200 °C) and hydrothermal time (24 h) were favorable for the synthesis of TiO_2 particles;
(3) Low calcination temperature (200 °C) was sufficient to reduce the organic residues on TiO_2 surfaces. High calcination temperature (>450 °C) would damage the surface morphology and crystal structure of TiO_2, which caused the reduction of NO conversion efficiency;
(4) under the optimal conditions (hydrothermal condition: 200 °C for 24 h, calcination temperature: 200 °C), the photocatalytic efficiency of catalyst would reach around 60% higher than that of Degussa P25.

Acknowledgement

This project was financially supported by the New Century Excellent Scholar Program of Ministry of Education of China (NCET-04-0549).

References

[1] Y.G. Adewuyi, S.O. Owusu, Aqueous absorption and oxidation of nitric oxide with ozone for the treatment of tail gases: process feasibility, stoichiometry, reaction pathways, and absorption rate, Ind. Eng. Chem. Res. 42 (2003) 4084–4100.
[2] M. Radojevic, Reduction of nitrogen oxides in flue gases, Environ. Pollut. 102 (1998) 685–689.
[3] J.M. Beér, Combustion technology developments in power generation in response to environmental challenges, Prog. Energy Combust. Sci. 26 (2000) 301–327.
[4] A.M. Efstathiou, K. Fliatoura, Selective catalytic reduction of nitric oxide with ammonia over V_2O_5/TiO_2 catalyst: a steady-state and transient kinetic study, Appl. Catal. B: Environ. 6 (1995) 35–39.
[5] H. Miessner, K.-P. Francke, R. Rudolph, Th. Hammer, NOx removal in excess oxygen by plasma-enhanced selective catalytic reduction, Catal. Today 75 (2002) 325–330.
[6] R.M. Heck, Catalytic abatement of nitrogen oxides—stationary applications, Catal. Today 53 (1999) 519–523.
[7] H. Takeuchi, M. Ando, N. Kizawa, Absorption of nitrogen oxides in aqueous sodium sulfite and bisulfite solutions, Ind. Eng. Chem. Proc. Des. Dev. 16 (1977) 303–308.
[8] L. Chen, J.-W. Lin, C.-L. Yang, Absorption of NO_2 in a packed tower with Na_2SO_3 aqueous solution, Environ. Prog. 21 (2002) 225–230.
[9] C.H. Shen, G.T. Rochelle, Nitrogen dioxide absorption and sulfite oxidation in aqueous sulfite, Environ. Sci. Technol. 32 (1998) 1994–2003.
[10] S. Barman, L. Philip, Integrated system for the treatment of oxides of nitrogen from flue gases, Environ. Sci. Technol. 40 (2006) 1035–1041.
[11] A.L. Linsebigler, G.Q. Lu, J.T. Yates Jr., Photocatalysis on TiO_2 surfaces: principles, mechanisms, and selected results, Chem. Rev. 95 (1995) 735–758.
[12] J. Zhao, X.D. Yang, Photocatalytic oxidation for indoor air purification: a literature review, Build. Environ. 38 (2003) 645–654.
[13] T. Ibusuki, K. Takeuchi, Removal of low concentration of nitrogen oxides through photoassisted heterogeneous catalysis, J. Mol. Catal. 88 (1994) 93–102.
[14] H. Ichiura, T. Kitaoka, H. Tanaka, Photocatalytic oxidation of NOx using composite sheets containing TiO_2 and a metal compound, Chemosphere 51 (2003) 855–860.
[15] J.S. Dalton, P.A. Janes, N.G. Jones, J.A. Nicholson, K.P. Hallam, G.C. Allen, Photocatalytic oxidation of NOx gases using TiO2: a surface spectroscopic approach, Environ. Pollut. 120 (2002) 415–422.

[16] K. Hashimoto, K. Wasada, M. Osaki, E. Shono, K. Adachi, N. Toukai, H. Kominami, Y. Kera, Photocatalytic oxidation of nitrogen oxide over titania-zeolite composite catalyst to remove nitrogen oxides in the atmosphere, Appl. Catal. B: Environ. 30 (2001) 429–436.
[17] S. Devahasdin, C. Fan Jr., K. Li, D.H. Chen, TiO_2 photocatalytic oxidation of nitric oxide: transient behavior and reaction kinetics, J. Photochem. Photobiol. A 156 (2003) 161–170.
[18] K. Byrappa, M. Yoshimura, Handbook of Hydrothermal Technology—a Technology for Crystal Growth and Materials, Noyes Publications, Park Ridge, New Jersey, USA, 2001, pp. 717–729.
[19] X.Y. Deng, Y.H. Yue, Z. Gao, Gas-phase photo-oxidation of organic compounds over nanosized TiO_2 photocatalysts by various preparations, Appl. Catal. B: Environ. 39 (2002) 135–147.
[20] A.I. Kontos, I.M. Arabatzis, D.S. Tsoukleris, A.G. Kontos, M.C. Bernard, D.E. Petrakis, P. Falaras, Efficient photocatalysts by hydrothermal treatment of TiO_2, Catal. Today 101 (2005) 275–281.
[21] C.Y. Wu, Y.H. Yue, X.Y. Deng, W.M. Hua, Z. Gao, Investigation on the synergetic effect between anatase and rutile nanoparticles in gas-phase photocatalytic oxidations, Catal. Today 93–95 (2004) 863–869.
[22] H.Q. Wang, Z.B. Wu, W.R. Zhao, B.H. Guan, Photocatalytic oxidation of nitrogen oxides using TiO_2 loading on woven glass fabric, Chemosphere 66 (2007) 185–190.
[23] M. Hirano, C. Nakahara, K. Ota, O. Tanaike, M. Inagaki, Photoactivity and phase stability of ZrO_2-doped anatase-type TiO_2 directly formed as nanometer-sized particles by hydrolysis under hydrothermal conditions, J. Solid State Chem. 170 (2003) 39–47.
[24] J.G. Yu, G.H. Wang, B. Cheng, M.H. Zhou, Effects of hydrothermal temperature and time on the photocatalytic activity and microstructures of bimodal mesoporous TiO_2 powders, Appl. Catal. B: Environ. 69 (2006) 171–180.
[25] J.C. Yu, J.G. Yu, W.K. Ho, Z.T. Jiang, L.Z. Zhang, Effects of F^- doping on the photocatalytic activity and microstructures of nanocrystalline TiO_2 powders, Chem. Mater. 14 (2002) 3808–3816.
[26] J. Ovenstone, Preparation of novel titania photocatalysts with high activity, J. Mater. Sci. 36 (2001) 1325–1329.
[27] S.Y. Chae, M.K. Park, S.K. Lee, T.Y. Kim, S.K. Kim, W.I. Lee, Preparation of size-controlled TiO_2 nanoparticles and derivation of optically transparent photocatalytic film, Chem. Mater. 15 (2003) 3326–3331.
[28] M. Lazzeri, A. Vittadini, A. Selloni, Structure and energetics of stoichiometric TiO_2 anatase surfaces, Phys. Rev. B 63 (2001) 155409-1–155409-9.
[29] M. Toyoda, Y. Nanbu, Y. Nakazawa, M. Hirano, M. Inagaki, Effect of crystallinity of anatase on photoactivity for methyleneblue decomposition in water, Appl. Catal. B: Environ. 49 (2004) 227–232.
[30] H. Kominami, T. Matsuura, K. Iwai, B. Ohtani, S.-I. Nishimoto, Y. Ker, Ultra-highly active titanium(IV) oxide photocatalyst prepared by hydrothermal crystallization from titanium(IV) alkoxide in organic solvents, Chem. Lett. 24 (1995) 693–694.
[31] C.H. Cho, M.H. Han, D.H. Kim, D.K. Kim, Morphology evolution of anatase TiO_2 nanocrystals under a hydrothermal condition (pH 9.5) and their ultra-high photo-catalytic activity, Mater. Chem. Phys. 92 (2005) 104–111.
[32] F.B. Li, X.Z. Li, C.H. Ao, M.F. Hou, S.C. Lee, Photocatalytic conversion of NO using TiO_2-NH_3 catalysts in ambient air environment, Appl. Catal. B: Environ. 54 (2004) 275–283.